J. Fluid Mech. (2002), *vol.* 461, *pp.* 155–182.
DOI: 10.1017/S0022112002008285 Printed in the United Kingdom

Scalar probability density function and fine structure in uniformly sheared turbulence

By M. FERCHICHI AND S. TAVOULARIS

Department of Mechanical Engineering, University of Ottawa, Ottawa, Canada K1N 6N5

(Received 19 March 2001 and in revised form 27 December 2001)

This study is an experimental investigation of the probability density function (p.d.f.) and the fine structure of temperature fluctuations in uniformly sheared turbulence with a passively introduced uniform mean temperature gradient. The shear parameter was relatively large, resulting in vigorous turbulence production and a total mean strain up to 23. The turbulence Reynolds number was up to 253. The scalar fluctuations grew in a self-similar fashion and at the same exponential rate as the turbulence stresses, in conformity with predictions based on an analytical solution of the scalar variance equation. Analytical considerations as well as measurements demonstrate that the scalar p.d.f. is essentially Gaussian and that the scalar–velocity joint p.d.f. is essentially jointly Gaussian, with the conditional expectations of the velocity fluctuations linearly dependent on the scalar value. Joint statistics of the scalar and its dissipation rate indicate a statistical independence of the two parameters. The fine structure of the scalar was invoked from statistics of derivatives and differences of the scalar, in both the streamwise and transverse directions. Probability density functions of scalar derivatives and differences in the dissipative and the inertial ranges were strongly non-Gaussian and skewed, displaying flared, asymmetric tails. All measurements point to a highly intermittent scalar fine structure, even more intermittent than the fine structure of the turbulent velocity.

1. Introduction

The study of the fine structures of the velocity field and of transported scalars, such as temperature and concentration of contaminants, have long occupied a central place in turbulence research, due both to their importance in a variety of technological applications and to the key role that they play in the understanding of turbulence. A common theme in most of these studies is the theory of local isotropy, first presented for a velocity field by Kolmogorov (1941) and for a passive scalar advected by turbulence by Obukhov (1949) and Corrsin (1951). Although this theory has been remarkably successful in providing scaling laws for the fine structure, some of its predictions have been found to disagree with the experimental evidence. A hypothesis to explain such discrepancies attributes them to the 'spottiness' of the fine structure, a phenomenon referred to as 'internal intermittency'. During the past few decades, several theoretical arguments have been put forward to quantify internal intermittency and to devise corrections to Kolmogorov's predictions (e.g. Frisch 1995), but the issue does not appear to have been settled. The verification of these corrections relies heavily on comparisons with specially conceived experiments.

The study of passive scalar mixing is, experimentally, more accessible than that of momentum mixing, due to the simpler forms of scalar properties, compared

to corresponding velocity properties. For example, the rate of destruction of scalar fluctuations by molecular mixing, commonly referred to as 'scalar dissipation rate' has only three components, compared to the 12 independent components of the turbulent kinetic energy dissipation rate. Notwithstanding the qualitative similarities between the fine structures of the velocity and scalar fields, it has been found that the scalar field is generally 'more intermittent' than the velocity field in both the dissipative and the inertial spectral ranges. This is clearly demonstrated by the fact that the flatness of the streamwise scalar derivative is significantly larger than the flatness of the corresponding velocity derivative and has a stronger dependence on the Reynolds number (Sreenivasan & Antonia 1997). An indicator of the local anisotropy of scalar fields is the significant skewness in their streamwise derivatives, a phenomenon explained by the presence of large-scale, ramp-like structures (Gibson, Friehe & McConnell 1977; Sreenivasan, Antonia & Britz 1979; Sreenivasan & Tavoularis 1980; Tavoularis & Sreenivasan 1981). The skewness and flatness of transverse derivatives of the scalar have also been measured in different homogeneous and inhomogeneous flows (Sreenivasan, Antonia & Danh 1977; Tavoularis & Corrsin 1981*b*; Thoroddsen & Van Atta 1992; Tong & Warhaft 1994; and Mydlarski & Warhaft 1998). The skewness in these flows was found to be non-zero, in disagreement with local isotropy. Holzer & Siggia (1994) attributed this non-zero skewness to sharp scalar fronts, which they called a 'ramp-cliff' structure. This structure has also been confirmed numerically by Pumir (1994) and experimentally by Tong & Warhaft (1994). The local anisotropy of the scalar field at moderate Reynolds numbers has also been demonstrated by the inequality of the different components of the scalar dissipation rate and the deviation of the measured scalar dissipation rate from its locally isotropic estimate (Sreenivasan *et al.* 1977; Tavoularis & Corrsin 1981*b*; Antonia & Browne 1986; Thoroddsen & Van Atta 1996; Mydlarski & Warhaft 1998). In shear flows, the scalar spectrum slope in the inertia range was found to deviate significantly from the locally isotropic slope of $-5/3$, even at relatively large Reynolds numbers, at which the streamwise velocity spectrum slope approached $-5/3$ (Sreenivasan 1991), although in grid-generated turbulence the opposite was observed (Jayesh, Tong & Warhaft 1994; Mydlarski & Warhaft 1998). On the other hand, Antonia *et al.* (1996, 1997) found that the second-order structure functions of the scalar and velocity at $Re_\lambda \leqslant 230$ had comparable variations, with their inertial ranges displaying a $2/3$-law dependence. Finally, Mydlarski & Warhaft (1998) concluded that the inertial range of the scalar field was more intermittent than that of the velocity field, based on the observation that, in the inertial range and for the same Reynolds number and separation distance, the probability density function (p.d.f.) of the streamwise difference of the velocity was less flared than that of the scalar.

Studies of passive scalar transport and mixing, as well as studies of chemical reactions and combustion in turbulent flows, have extensively used the p.d.f. approach, because, unlike the conventional moment-based formulations, the equations governing the p.d.f. of the scalar fluctuations do not require 'closure' models, other than those used for the velocity field (Pope 1985). A general conservation equation for the scalar p.d.f. may be derived following the approach introduced by Lundgren (1967). Under any conditions of the mean velocity and scalar fields, this equation includes a molecular diffusion term that potentially couples the fine structure and the large-scale features of a turbulent field, because it explicitly contains the expectation of the scalar dissipation rate conditional upon the scalar value (Dopazo & O'Brien 1974; Pope 1976; Dopazo 1976). This quantity was modelled based on the 'conditionally Gaussian' assumption (Dopazo & O'Brien 1974, 1975; Dopazo 1976), which makes

use of local isotropy, but, in these models, the scalar p.d.f. failed to relax to the Gaussian distribution. This was subsequently achieved by the use of the mapping closure technique (Chen, Chen & Kraichnan 1989; Gao 1991; Gao & O'Brien 1991; O'Brien & Jiang 1991; Valiño 1995). Measurements of the conditional expectation of the scalar dissipation in non-reacting, inhomogeneous, shear flows have been presented by Kailasnath, Sreenivasan & Saylor (1993), Anselmet, Djeridi & Fulachier (1991, 1994) and Mi, Antonia & Anselmet (1995). While Anselmet *et al.* (1994) suggested that the scalar dissipation was independent of the scalar fluctuations in regions where the scalar p.d.f. was Gaussian, Mi *et al.* (1995) argued that, for this to happen, the flow had to be locally isotropic as well. In a DNS study of homogeneous flows, Eswaran & Pope (1988) found that the long-time scalar dissipation rate was independent of the scalar. In contrast, Jayesh & Warhaft (1992) reported that, in grid-generated turbulence, the conditional expectation of scalar dissipation depended on the initial scalar field when a mean scalar gradient was imposed on the flow, but not when a uniform mean scalar field was considered.

In isotropic turbulence with a uniform mean scalar, the rate of change of the scalar p.d.f. depends solely on the conditional expectation of the scalar dissipation. However, when a mean scalar gradient is present, additional terms appear, that contain the expectation of velocity components conditional upon the scalar value. Although Sahay & O'Brien (1993) and Overholt & Pope (1996) have shown that such terms have an effect on the evolution of the scalar p.d.f., no measurements of conditional velocity statistics have been reported, with the exception of the results of Tong & Warhaft (1995). The effect of mean shear on the different terms of the scalar p.d.f. equation has not yet been investigated, either analytically or experimentally.

The Gaussianity, or non-Gaussianity, of the scalar p.d.f. remains a controversial issue. While earlier studies (Tavoularis & Corrsin 1981*a*; Kerr 1985; Eswaran & Pope 1988; and others) confirmed Gaussianity, measurements in thermal convection at high Rayleigh numbers by Castaing *et al.* (1989) showed temperature fluctuations with p.d.f. having exponential tails in the so-called 'hard turbulence regime'. This result motivated others (Sinai & Yakhot 1989; Yakhot 1989; Valiño, Dopazo & Ros 1994) to obtain modelled solutions of a scalar p.d.f. that exhibited tails broader than Gaussian. Pumir, Shraiman & Siggia (1991) and Holtzer & Pumir (1993) developed a one-dimensional model which predicted exponential tails if the scalar were subject to a mean scalar gradient. The analytical studies prompted a renewed interest in measurements of passive scalar p.d.f., which, however, intensified the controversy. While Gollub *et al.* (1991) and Jayesh & Warhaft (1991, 1992) measured exponential tails when the Reynolds number exceeded a transition value, Thoroddsen & Van Atta (1992) and Mydlarski & Warhaft (1998) reported scalar p.d.f. that were nearly Gaussian. Furthermore, Kerstein & McMurtry (1994) showed that the form of the scalar p.d.f. depended strongly on the statistics of the advecting velocity field and Ching & Tsang (1997) found that the scalar p.d.f. had exponential tails even when the mean scalar gradient was zero and that the shape of the scalar p.d.f. depended on the ratio of diffusion time to velocity correlation time. Jaberi *et al.* (1996) applied a linear eddy model in stationary turbulence as well as DNS in decaying and forced turbulence and found that the p.d.f. of the scalar depended greatly on the initial conditions: when the initial scalar integral length scales were larger than the initial velocity integral scales or when the initial scalar field had a large proportion of small-scale contributions, the scalar p.d.f. would evolve towards distributions flatter than Gaussian. Moreover, the same DNS showed that a linear mean scalar field was not a sufficient condition for a non-Gaussian scalar p.d.f. to occur even at Reynolds

numbers larger than that suggested by Jayesh & Warhaft (1991, 1992). The same conclusions were also reached by Overholt & Pope (1996) in a DNS study of a passive scalar subjected to a mean scalar gradient in isotropic, stationary turbulence. Most recently, Warhaft (2000) argued that the reason for the absence of exponential tails in the scalar p.d.f. in the studies mentioned above is that their flow widths were not large enough to allow extreme scalar excursions to occur.

In summary, the literature contains a substantial number of experimental studies of the fine structure of scalars in turbulent flows. Many of these studies have been conducted in grid-generated turbulence, without or with a mean scalar gradient. The former case contains no production mechanism for either the velocity or the scalar fluctuations, and thus both decay. The latter case contains a production mechanism for scalar fluctuations, but not for the turbulent kinetic energy; consequently, the scalar field would probably evolve differently from the velocity field, which complicates a comparison of the corresponding fine structures. A number of other studies of scalar mixing have been conducted in different free and bounded shear flows. While such studies have undoubtedly produced many useful results, they are also complicated by their inherent inhomogeneity and by differences in the mechanisms of production and evolution of the velocity and scalar fields. All these problems may be avoided by considering the case of uniformly sheared, nearly homogeneous turbulence with a uniform mean scalar gradient, in which the turbulent kinetic energy and the scalar variance have similar balance equations and should grow at comparable rates. This configuration has been studied in detail experimentally by Tavoularis & Corrsin (1981*a*, *b*, hereafter referred to as TC), who have presented moments, correlations, spectra and p.d.f.s of the scalar and its derivatives, as well as addressed the issue of local isotropy. Their results have been used extensively in many different contexts; however, since they were collected, more than two decades ago, a number of new issues and controversies have risen, which TC could not have anticipated. The present experiments have been conducted in a flow which is, in broad terms, the same as that in the TC experiments. However, in view of the previous experience, a number of improvements have been introduced. In particular, in the present flow, the initial scalar field has been decoupled from the initial velocity field by the use of a heating screen inserted in the developed part of the flow. The evolutions of the scalar moments and correlations in the present flow have been documented and compared with the TC results. Emphasis has been placed on the fine structure and the p.d.f. of the scalar, including statistics of scalar differences in the inertial range. The present paper also contains analyses of the evolutions of the scalar variance and p.d.f., based on the corresponding governing equations. It is hoped that the present results will contribute to the understanding of scalar mixing in shear flows and will help resolve some of the surrounding controversies.

2. Analytical results

2.1. *Self-similar evolution of the scalar field*

Consider a stationary, transversely homogeneous, uniformly sheared turbulent flow, with a mean velocity gradient $\mathrm{d}\bar{U}_1/\mathrm{d}x_2$. Then, the turbulent kinetic energy equation is simplified to (TC)

$$\bar{U}_1 \frac{\mathrm{d}(\frac{1}{2}q^2)}{\mathrm{d}x_1} = P - \epsilon, \tag{1}$$

where the turbulent kinetic energy per unit mass is $\frac{1}{2}q^2 = \frac{1}{2}\overline{u_i u_i}$, its production rate is $P = -\overline{u_1 u_2}\,\mathrm{d}\bar{U}_1/\mathrm{d}x_2$ and its dissipation rate is ϵ. Tavoularis (1985) has shown that, under such conditions, there is a self-similar, asymptotic development state in which all relevant dimensionless ratios remain constant and all Reynolds stresses, as well as q^2, grow exponentially, for example (see also Tavoularis & Karnik 1989)

$$q^2 = q_r^2 \exp(\kappa(\tau - \tau_r)), \tag{2}$$

and

$$u_i'^2 = u_{ir}^2 \exp(\kappa(\tau - \tau_r)), \tag{3}$$

where the subscript r denotes values at a reference position within the asymptotic state, the total strain is defined as $\tau = (x_1/\bar{U}_1)\,\mathrm{d}\bar{U}_1/\mathrm{d}x_2$ and the dimensionless coefficient κ is defined

$$\kappa = -\frac{\overline{u_1 u_2}}{q^2}\left(1 - \frac{\epsilon}{P}\right). \tag{4}$$

Further, consider the above flow with a passively superimposed, stationary random scalar field having a uniform mean gradient $\mathrm{d}\bar{T}/\mathrm{d}x_2$ and transversely uniform fluxes $\overline{\theta u_i}$, $i = 1, 2, 3$. Then (TC), the equation governing the mean squared scalar fluctuations, θ'^2 (primes indicate standard deviations), may be simplified to

$$\bar{U}_1 \frac{\mathrm{d}(\frac{1}{2}\theta'^2)}{\mathrm{d}x_1} = P_\theta - \chi, \tag{5}$$

where the rate of production of the scalar fluctuations is $P_\theta = -\overline{\theta u_2}\,\mathrm{d}\bar{T}/\mathrm{d}x_2$ and their mean rate of dissipation is $\chi = \gamma\overline{(\partial\theta/\partial x_i)(\partial\theta/\partial x_i)}$, with γ being the molecular diffusivity, or thermal diffusivity. Extending Tavoularis' (1985) analysis to include the scalar field, one may consider a self-similar, asymptotic state, in which all relevant dimensionless ratios for the scalar, including the correlation coefficient $\rho_{2\theta} = \overline{\theta u_2}/\theta' u_2'$ and the ratio χ/P_θ, are constant. Then, it is easy to show that the solution of equation (5) is

$$\theta'^2 = \theta_r^2 \exp(\kappa(\tau - \tau_r)) \tag{6}$$

where the reference temperature θ_r is

$$\theta_r = \frac{-4\rho_{2\theta} u_{2r}(\mathrm{d}\bar{T}/\mathrm{d}x_2)(1 - \chi/P_\theta)}{\kappa\,\mathrm{d}\bar{U}_1/\mathrm{d}x_2}. \tag{7}$$

This demonstrates that the scalar variance should grow asymptotically at the same rate as the Reynolds stresses. Its value should also be independent of the initial level of the scalar fluctuations, so that the scalar field would be entirely determined by the mean velocity gradient, the initial Reynolds stress level, the mean scalar gradient, and the (possibly universal) values of the dimensionless ratios $\rho_{2\theta}$ and χ/P_θ.

Finally, if the scalar field were locally isotropic, its mean destruction rate would be

$$\chi_{li} = 6\gamma\frac{\theta'^2}{\lambda_{\theta 1}^2};$$

then it follows that the Corrsin microscale $\lambda_{\theta 1}$ must be independent of x_1. Following Tavoularis' (1985) comments on the Taylor microscale λ, one may show that $\lambda_{\theta 1}$ must vary in the x_2-direction to compensate for the transverse variation of $\bar{U}_1$ in equation (5).

2.2. *A balance equation for the scalar p.d.f.*

Following Lundgren's (1967) approach, one may define the p.d.f. of a random scalar function of position and time, $\theta(x_i, t)$, as

$$p(\psi, x_i, t) = \langle \delta[\theta(x_i, t) - \psi] \rangle, \tag{8}$$

where ψ is the scalar space, δ is Dirac's delta function and the brackets $\langle\,\rangle$ indicate ensemble averaging. An equation for the evolution of the p.d.f. may be obtained by taking the time derivative of equation (8) and substituting the quantity $\partial\theta/\partial t$ by its balance from the equation governing the scalar fluctuations. Without further assumptions, but after a number of statistical manipulations, one may obtain the general equation for the scalar p.d.f. as

$$\frac{\partial p}{\partial t} + \bar{U}_j \frac{\partial p}{\partial x_j} = -\frac{\partial(\langle u_j|\theta = \psi\rangle p)}{\partial x_j} - \frac{\partial \overline{\theta u_j}}{\partial x_j}\frac{\partial p}{\partial \psi} + \frac{\partial \bar{T}}{\partial x_j}\frac{\partial(\langle u_j|\theta = \psi\rangle p)}{\partial \psi} - \frac{\partial^2(\langle \epsilon_\theta|\theta = \psi\rangle p)}{\partial \psi^2} + \gamma \frac{\partial^2 p}{\partial x_j \partial x_j}. \tag{9}$$

Details for the derivation of equation (9), not readily available in published references, may be found in the dissertation by Ferchichi (2000). In this equation, $\langle u_j|\theta = \psi\rangle$ and $\langle \epsilon_\theta|\theta = \psi\rangle$ denote, respectively, the expectations of the velocity fluctuations and of the fluctuating scalar destruction rate, $\epsilon_\theta = \gamma(\partial\theta/\partial x_i)(\partial\theta/\partial x_i)$, conditional upon the scalar value. The different terms in equation (9) may be assigned the following physical significance.

left-hand side: total rate of change of the p.d.f.;
1st term, right-hand side: turbulent transport of the p.d.f. in physical space;
2nd term, right-hand side: transport of the p.d.f. by gradients of the turbulent fluxes;
3rd term, right-hand side: turbulent transport of the p.d.f. in probability space;
4th term, right-hand side: molecular diffusion of the p.d.f. in probability space;
last term, right-hand side: molecular diffusion of p.d.f. in physical space.

For a turbulent flow and a scalar field satisfying the conditions outlined in the previous section, the scalar p.d.f. would be independent of x_2, x_3 and t, and equation (9) may be simplified to

$$\bar{U}_1 \frac{\partial p}{\partial x_1} = -\frac{\partial(\langle u_1|\theta = \psi\rangle p)}{\partial x_1} - \frac{\mathrm{d}\overline{\theta u_1}}{\mathrm{d}x_1}\frac{\partial p}{\partial \psi} + \frac{\mathrm{d}\bar{T}}{\mathrm{d}x_2}\frac{\partial(\langle u_2|\theta = \psi\rangle p)}{\partial \psi} - \frac{\partial^2(\langle \epsilon_\theta|\theta = \psi\rangle p)}{\partial \psi^2} + \gamma \frac{\partial^2 p}{\partial x_1^2}. \tag{10}$$

2.3. *Gaussianity of the scalar p.d.f.*

At first, let us explore the admissibility of the Gaussian p.d.f. as a solution of equation (10). Let $g(\eta)$ represent the standard Gaussian function $g(\eta) = (1/\sqrt{2\pi})\mathrm{e}^{-\eta/2}$. Then, a Gaussian, self-preserving scalar p.d.f. for a stationary, transversely homogeneous flow must have the form

$$p(\psi, x_1) = \frac{1}{\theta'(x_1)} g(\eta), \tag{11}$$

where $\eta = \psi/\theta'(x_1)$. Further, assume that the conditional expectations of u_1 and u_2 are linearly related to the value of the scalar, namely that

$$\langle u_i|\theta = \psi\rangle = \rho_{i\theta} u_i' \eta, \tag{12}$$

and that the scalar dissipation rate is independent of the value of the scalar, such that

$$\langle \epsilon_\theta | \theta = \psi \rangle = \chi. \tag{13}$$

Notice that the above assumptions would be satisfied by pairs of (u_i, θ) and $(\epsilon_\theta, \theta)$ that are jointly Gaussian (the latter pair must also be uncorrelated), but also by more general classes of joint p.d.f. Substituting the above results into equation (10) and performing some simple algebraic manipulations, one may derive the equation

$$\left[\bar{U}_1 \frac{\mathrm{d}(\frac{1}{2}\theta'^2)}{\mathrm{d}x_1} - P_\theta + \chi\right](1-\eta^2) + 3\rho_{i\theta}u_i'\eta\frac{\mathrm{d}(\frac{1}{2}\theta'^2)}{\mathrm{d}x_1} + \gamma\left[-\theta'\frac{\mathrm{d}^2\theta'}{\mathrm{d}x_1^2} + 2\left(\frac{\mathrm{d}\theta'}{\mathrm{d}x_1}\right)^2\right] = 0. \tag{14}$$

In this expression, it is easy to see that the second term would be of lower order of magnitude than the mean convection term; in the present experiments, the ratio of these two terms is less than 5.7% for $\eta < 0.62$ and $\eta > 1.62$; the fact that the first term vanishes at $\eta = 1$ is not of concern in an order-of-magnitude analysis. Furthermore, for large Reynolds number, the last term would also be negligible; in the present experiments, its ratio to the mean convection term is $8.4 \times 10^{-8}/(1-\eta^2)$, which is indeed negligible, except in the near vicinity of $\eta = 1$. Then, equation (14) would be reduced to equation (5), which is satisfied within the present approximation. In conclusion, under the current approximations and conditions, a Gaussian p.d.f. satisfies the scalar p.d.f. equation in uniformly sheared turbulence with a uniform mean scalar gradient.

In view of the above analysis, and with the use of direct experimental evidence, one can prove that the Gaussian p.d.f. is the only solution of equation (10), within the present context. First, one may omit the first, second and last terms on the right-hand side of equation (10) by comparison to the left-hand side, by direct substitution of experimental values and without the need for further assumptions. Then, the p.d.f. equation may be further simplified to

$$\bar{U}_1\frac{\partial p}{\partial x_1} = \frac{\mathrm{d}\bar{T}}{\mathrm{d}x_2}\frac{\partial(\langle u_2|\theta=\psi\rangle p)}{\partial\psi} - \frac{\partial^2(\langle\epsilon_\theta|\theta=\psi\rangle p)}{\partial\psi^2}. \tag{15}$$

This equation is analogous to equation (5) for the scalar variance. However, due to the conditional expectations appearing in it, it cannot be solved for the p.d.f. without further assumptions. The desired solution must be self-similar, which implies that

$$p(\psi, x_1) = \frac{1}{\theta'(x_1)}f(\eta), \tag{16}$$

where $f(\eta)$ is a function of $\eta = \psi/\theta'(x_1)$. Once more resorting to the experimental evidence, one may use expressions (12) and (13) and some simple algebraic manipulations to transform equation (15) into the form

$$\frac{\mathrm{d}^2 f}{\mathrm{d}\eta^2} + \eta\frac{\mathrm{d}f}{\mathrm{d}\eta} + f = 0, \tag{17}$$

which has the general solution

$$f(\eta) = c_1 e^{-\frac{1}{2}\eta^2}\int_0^\eta \mathrm{e}^{t^2/2}\mathrm{d}t + c_2\mathrm{e}^{-\eta^2/2}. \tag{18}$$

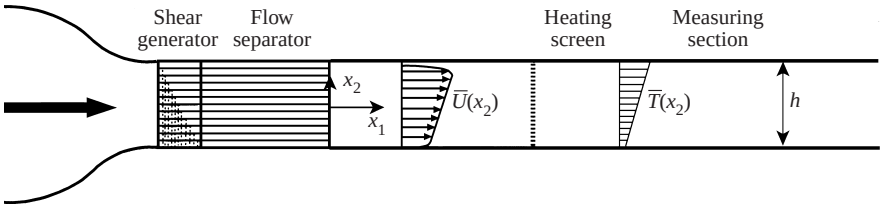

FIGURE 1. Sketch of the wind tunnel test section illustrating the shear generator and the heating system.

Both terms in this expression vanish as $\eta \to \pm\infty$ (Abramowitz & Stegun, 1972), but the first term does so more slowly than the second term, irrespectively of the values of the constants c_1 and c_2. Therefore, if $c_1 > 0$, $f(\eta)$ would become negative as $\eta \to -\infty$, which is impossible for a p.d.f. Similarly, if $c_1 < 0$, $f(\eta)$ would become negative as $\eta \to +\infty$. Thus, the only acceptable value is $c_1 = 0$. Finally, in order to satisfy the p.d.f. requirement $\int_{-\infty}^{\infty} f(\eta)\mathrm{d}\eta = 1$, one must have $c_2 = 1/\sqrt{2\pi}$. In conclusion, the only acceptable solution of equation (17) is the Gaussian function.

3. Experimental facility and instrumentation

The experiments were conducted in a wind tunnel, which is sketched in figure 1. The mean shear was produced by a shear generator (Karnik & Tavoularis 1987), installed immediately following the 16:1 contraction, and comprising a set of 12 separate channels, each 25.4 mm high, separated by aluminium plates, 1.6 mm thick and 150 mm long. One or more strips of screens with various mesh sizes and solidities were stretched across each channel and adjusted to produce a uniform shear. A flow separator, consisting of 12 parallel plates, 610 mm long and aligned with those of the shear generator, was inserted into the flow in order to make the larger scales of the flow uniform on the transverse plane. The test section had a height of $h = 305$ mm, a nominal width of 457 mm wide and a length of 5180 mm. The sidewalls of the downstream half of the test section diverged slightly to compensate for boundary layer growth.

The heating system was mounted on a wooden frame that was inserted normal to the flow at a position 792 mm (2.6h) downstream from the exit of the flow separator, which was taken as the origin of the x_1-axis. It consisted of 47 heating ribbons (Nicrome 60), stretched horizontally across the frame with the use of springs. These ribbons were 0.8 mm wide, 0.08 mm thick and 6.3 mm apart from each other; electric current was supplied to each pair connected in series by an individual variable transformer which was adjusted to produce the desired mean temperature profile. A thin copper plate, machined into thin strips separated by insulated sections, was epoxied to the top wall of the test section and was heated electrically to the local mean temperature; this prevented heat losses from the warmer part of the flow and thus eliminated the thermal boundary layer from the top wall and improved the uniformity of the mean temperature gradient. To further minimize heat losses, the test section was insulated using fibreglass sheets.

The velocity fluctuations were measured using a specially made, sub-miniature cross-wire probe, with sensors having a diameter of 5 μm, a length of 0.7 mm and a nominal distance of about 1 mm. Their outputs were corrected for temperature variations, using the cold-wire signal. The mean temperature of the heated flow was measured by glass-coated, thermistor mini-probes (Fenwal Electronics, 2000).

Temperature fluctuations were measured with cold-wire probes, with sensors made of 1 μm diameter, 100% platinum wire, and having a typical length of about 0.5 mm. For the measurement of temperature–velocity correlations, a separate cold wire was positioned next to the cross-wire probe, at a distance of about 1 mm from the nearest hot wire. Transverse temperature derivatives and differences were measured by a pair of parallel cold wires with adjustable transverse separation distances. For the transverse derivatives, the two sensors were separated by about 0.5 mm. All cold wires were operated by home-made, constant-current, electronic circuits, powered by dry cell batteries to minimize the electronic noise and the power line frequency contamination of the signals. At the current of 0.4 mA used, the cold wires showed a negligible sensitivity to velocity.

The hot-wire signals were low-pass filtered at a cut-off frequency of 8 kHz (3 dB point), the cold-wire signal was low-pass filtered at 10 kHz and all signals were digitized simultaneously at a frequency of 20 kHz, using a 16-bit analog-to-digital converter (IOTECH, 488/16). The discretized cold-wire signals were further low-pass filtered using a non-recursive, zero-phase-shift, digital filter at a cut-off frequency of 5 kHz prior to processing. At this cut-off frequency, the signal-to-noise ratio varied from 47 to about 90. To ensure a good statistical representation of the large scales of the flow, 60 records of 262 144 data points were collected.

Streamwise derivatives and differences were evaluated using Taylor's 'frozen flow' approximation. The streamwise Taylor and Corrsin microscales were, respectively, calculated as

$$\lambda_{11} = \bar{U}_1[\overline{u_1^2}/\overline{(\partial u_1/\partial t)^2}]^{1/2}, \quad \lambda_{\theta 1} = \bar{U}_1[2\overline{\theta^2}/\overline{(\partial \theta/\partial t)^2}]^{1/2},$$

while the transverse Corrsin microscale was measured as

$$\lambda_{\theta 2} = [2\overline{\theta^2}/\overline{(\partial \theta/\partial x_2)^2}]^{1/2}.$$

The scalar dissipation rate was evaluated from its streamwise component (Kailasnath *et al.* 1993; Jayesh & Warhaft 1992). Typical values of the Taylor and Corrsin microscales were $\lambda_{11} = 5.2$ mm, $\lambda_{\theta 1} = 4.6$ mm and $\lambda_{\theta 2} = 3.0$ mm throughout the measuring range, while the Kolmogorov microscale η was found to decrease from about 0.20 mm to about 0.17 mm along the measuring section. The Kolmogorov frequency for convection of turbulence eddies, $f_K = \bar{U}_1/2\pi\eta$, increased from about 5.2 kHz to about 6.2 kHz. The Corrsin–Obukhov microscale, corresponding to the dissipative scales of the temperature variance and defined as $\eta_\theta = \eta\,\mathrm{Pr}^{-3/4}$, decreased from about 0.23 mm to about 0.21 mm. Accordingly, the Kolmogorov frequency for temperature fluctuations, $f_{K\theta} = \bar{U}_1/2\pi\eta_\theta$, increased from about 4.0 kHz to about 4.9 kHz.

The mean-square temperature derivative was corrected for the averaging effect of a finite-length sensor. This correction, estimated using the results of Wyngaard (1971), was, in the worst case, about 10%, which resulted in a downward correction to the Corrsin microscale by about 5%. Another possible source of contamination of cold-wire measurements is heat conduction to the supports. This effect is negligible for sensor length-to-diameter ratios larger than 1500 (Browne & Antonia 1987). For the present 1 μm sensors, this would require a length of 1.5 mm, which would result in an error, due to the finite length effect, of about 38% in estimating the mean-square derivative (Wyngaard 1971). Further reducing the diameter of the cold wire would make it very fragile and extremely hard to handle and repair, particularly for pure platinum sensors. For this reason, and in view of the fact that it is the spatial resolution of the cold wire, and not conduction to supports, that makes the

predominant contribution to the uncertainty in estimating temperature derivative statistics (Mydlarski & Warhaft 1998), the length-to-diameter ratio of about 500 used here was considered to be a good compromise. For a comparison, Mydlarski & Warhaft (1998) used a cold wire with a ratio of about 560. The cold-wire separation used for transverse derivative measurements was about $2\eta_\theta$, which is within the acceptable range (Antonia & Mi 1993; Anselmet *et al.* 1994; and Tong & Warhaft 1994).

4. Experimental results

4.1. *The mean fields*

In the absence of the heating system, the turbulent flow was essentially the same as that documented in earlier reports on uniformly sheared flow in the same facility (Tavoularis & Karnik 1989; Ferchichi & Tavoularis 2000). The use of the heating system caused a small pressure drop, which resulted in a reduction of the mean shear (see Karnik & Tavoularis 1987, for a detailed discussion of this effect). The heating elements also produced some additional turbulence, which was allowed to decay before the measuring section. The streamwise position of insertion of the heating system was far enough from the flow separator to permit flow development towards its asymptotic structure, and also far enough upstream to permit the growth of strong temperature fluctuations under the influence of the mean scalar gradient. It was observed that, for centreline speeds higher than about $7\,\mathrm{m\,s^{-1}}$, some heated ribbons started vibrating with audible sound ('singing'). For this reason, and due to power limitations of the electric transformers, the flow speed on the centreline of the tunnel was selected to be $U_c = 6.6\,\mathrm{m\,s^{-1}}$, while the mean temperature rise on the centreline was fixed at $\Delta T_c = 1.37$ K. This required heating of the ribbons at powers varying from about 5 W to about 720 W. Under such relatively low overheats, buoyancy effects were expected to be negligible so that temperature can be treated as a passive scalar. As an additional confirmation of scalar passivity, we have computed that both the flux and the gradient Richardson numbers were of the order of 10^{-4}, which is far too small for buoyancy to play any role in scalar fluctuation production (TC).

Figure 2(*a*) shows transverse profiles of the mean velocity at different downstream locations. These profiles displayed good linearity and downstream constancy in the core of the test section. The transverse mean velocity $\bar{U}_2$ varied between -1% and -4% of U_c. The mean shear was, typically, $\mathrm{d}\bar{U}_1/\mathrm{d}x_2 \approx 40\,\mathrm{s^{-1}}$ and the shear parameter, $k_s = (1/U_c)\mathrm{d}\bar{U}_1/\mathrm{d}x_2$, was $6.0 \pm 0.15\,\mathrm{m^{-1}}$, measurably lower than the value $7.1 \pm 0.19\,\mathrm{m^{-1}}$ in the absence of the heating system (Ferchichi & Tavoularis 2000). Typical transverse profiles of the mean temperature at different downstream locations are shown in figure 2(*b*). These profiles also displayed good linearity, with a nearly constant mean temperature gradient $\mathrm{d}\bar{T}/\mathrm{d}x_2 \approx 7.8\,\mathrm{K\,m^{-1}}$ in the core of the wind tunnel. A summary of experimental values in the present study and the TC experiments is provided in table 1. The total strain experienced by the flow is defined as $\tau = k_s x_1$.

A comparison of the two studies shows comparable mean shear rates but a much lower convection speed in the present work. This resulted in a significantly higher shear parameter in the present experiments, which implies more vigorous turbulence production. As a result, the total strain experienced by the turbulence within the present apparatus was $\tau_{max} = 23.0$, while the corresponding value in the TC experiments was merely $\tau_{max} = 12.6$. The turbulence intensity at the exit of the

Parameter	TC flow ($\tau = 12.6$)	Present flow ($\tau = 23.0$)
U_c (m s^{-1})	12.4	6.6
$d\bar{U}_1/dx_2$ (s^{-1})	46.8	39.6
k_s (m^{-1})	3.8	6.0
u_1'/U_c	0.056	0.114
u_2'/u_1'	0.55	0.58
$-\overline{u_1u_2}/u_1'u_2'$	0.45	0.45
$L_{11,1}$ (mm)	57	49
λ_{11} (mm)	5.8	5.2
$Re_\lambda = u_1'\lambda_{11}/\nu$	266	253
η (mm)	0.18	0.17
Heating system	rods	ribbons
Position of h.s.	$\tau = 0$	$\tau = 4.8$
ΔT_c (K)	1.50	1.37
$d\bar{T}/dx_2$ (K m^{-1})	9.5	7.8
$\theta'/\Delta T_c$	0.083	0.080
$\theta'/(d\bar{T}/dx_2)$ (m)	0.013	0.014
$\overline{\theta u_1}/\theta' u_1'$	0.59	0.56
$-\overline{\theta u_2}/\theta' u_2'$	0.45	0.50
$\lambda_{\theta 1}/\lambda_{11}$	0.88	0.88
$\lambda_{\theta 2}/\lambda_{\theta 1}$	0.73	0.66
$L_{\theta 1}/L_{11,1}$	0.76	0.74
η_θ (mm)	0.23	0.21
$(\chi/P_\theta)_{balance}$	0.81	0.80
$(\chi/P_\theta)_{direct}$	0.58	0.57
χ_{li}/P_θ	0.45	0.41

TABLE 1. Summary of measured parameters in the experiments of Tavoularis & Corrsin (1981*a*, *b*) and the present experiments.

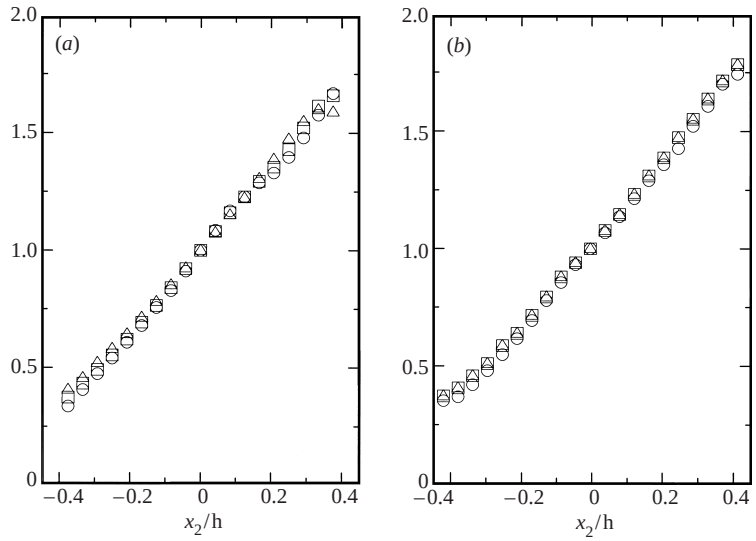

FIGURE 2. Transverse profiles of (*a*) the dimensionless mean velocity $\bar{U}_1/U_c$ and (*b*) the mean temperature $\bar{T}/\Delta T_c$ in the heated flow. $x_1/h = 7.6$ (○), 9.3 (□) and 12.6 (△).

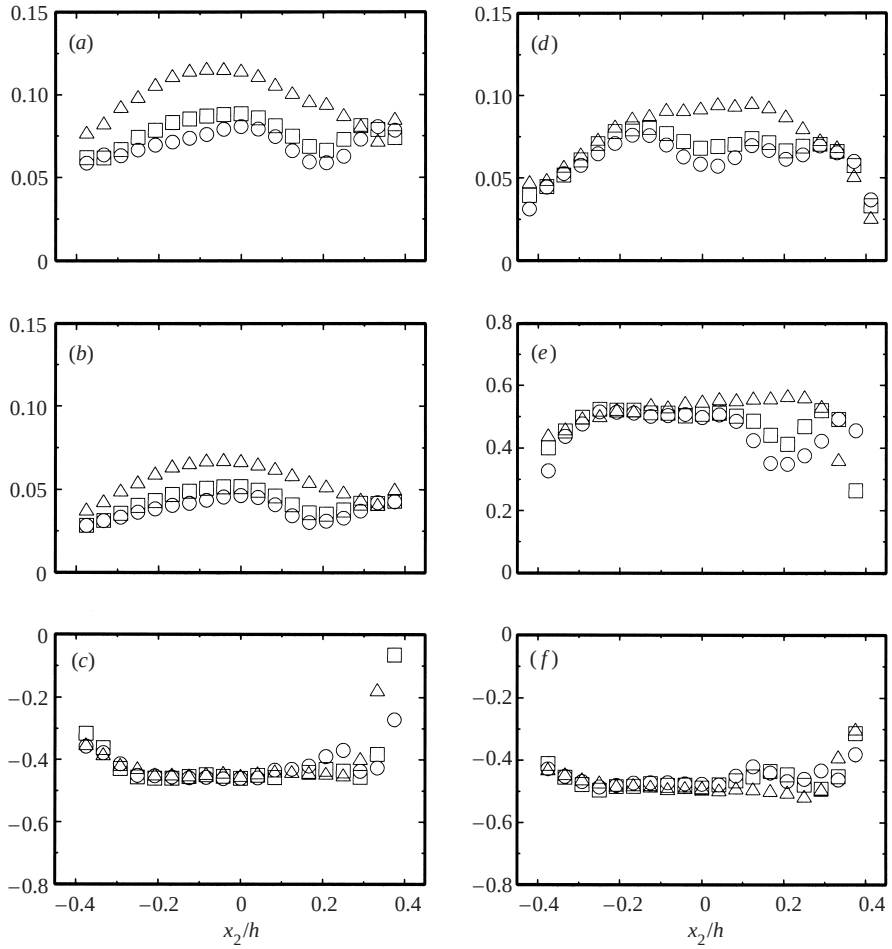

FIGURE 3. Transverse profiles of (*a*) u_1'/U_c, (*b*) u_2'/U_c, (*c*) $\overline{u_1u_2}/u_1'u_2'$, (*d*) $\theta'/\Delta T_c$, (*e*) $\overline{u_1\theta}/u_1'\theta'$ and (*f*) $\overline{u_2\theta}/u_2'\theta'$. $x_1/h = 7.6$ (○), 9.3 (□) and 12.6 (△).

present test section was twice as high as the TC value. Similar observations may be made for the mean scalar fields. Although the mean temperature rises and the mean temperature gradients were comparable in the two experiments, the differences in convection speeds also rendered the present scalar production mechanism nearly twice as vigorous.

4.2. *Moments and lengthscales*

A verification of the approximate transverse homogeneity of the velocity and scalar fields is provided in figure 3, which shows transverse profiles of the r.m.s. velocity and temperature fluctuations and the dominant shear stress and heat flux correlation coefficients at three representative downstream stations. The transverse variations of all parameters were less than $\pm 15\%$ in the central half of the wind tunnel cross-section, while, in some cases, the variations were considerably lower. The downstream evolutions of the two normal turbulent stresses and the temperature variance are shown in figure 4(*a*). Near the heating screen, its effect on the growth rate of the turbulence and, particularly, on that of the temperature fluctuations was noticeable, but, beyond a distance corresponding to a total strain increment of about 10

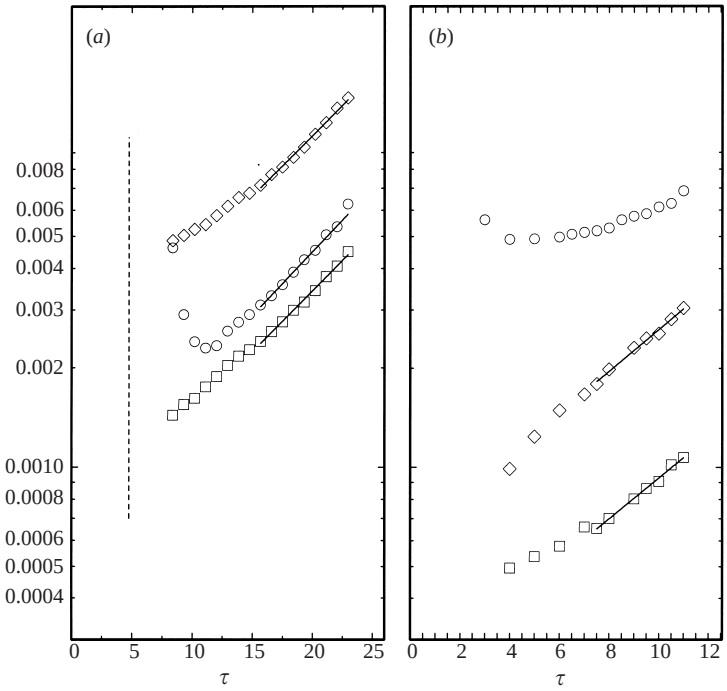

FIGURE 4. Downstream evolution of the dimensionless turbulent stresses and temperature fluctuations in (*a*) the present experiments and (*b*) the TC experiments. ◇, $\overline{u_1^2}/U_c^2$; □, $\overline{u_2^2}/U_c^2$; ○, $\overline{\theta^2}/\Delta T_c^2$; the dashed line in (*a*) indicates the location of the heating system, while solid lines in both parts indicate fitted exponential expressions.

($\tau > 15$), both the turbulence and the scalar fluctuations appeared to be dominated by production by the mean gradients and all second moments grew exponentially. Exponential expressions fitted independently to the measured evolutions of the two normal turbulent stresses for $15.7 < \tau < 23.0$ gave

$$\frac{\overline{u_1^2}}{U_c^2} = 0.00187\,\mathrm{e}^{0.0846\tau} \quad \text{and} \quad \frac{\overline{u_2^2}}{U_c^2} = 0.000631\,\mathrm{e}^{0.0846\tau},$$

showing that both grew at the same rate, which was somewhat slower than their growth rate in the absence of the heating system (Ferchichi & Tavoularis 2000). This difference may be attributed to the reduction in the shear parameter k_s from the higher value in the undisturbed shear flow, due to the pressure drop across the heating wire array (Karnik & Tavoularis 1987). The ratio of the rms velocities u_2'/u_1' measured here was close to the TC value (table 1).

The temperature variance for $15.7 < \tau < 23.0$ (figure 4*a*) was represented well by the fitted exponential expression

$$\frac{\overline{\theta^2}}{\Delta T_c^2} = 0.000771\,\mathrm{e}^{0.00882\tau}.$$

The temperature variance growth exponent was essentially the same (4% higher) as the exponent of the turbulent stresses, thus confirming that the scalar fluctuation field grew in a self-similar fashion that was imposed by the turbulence and according to equation (6).

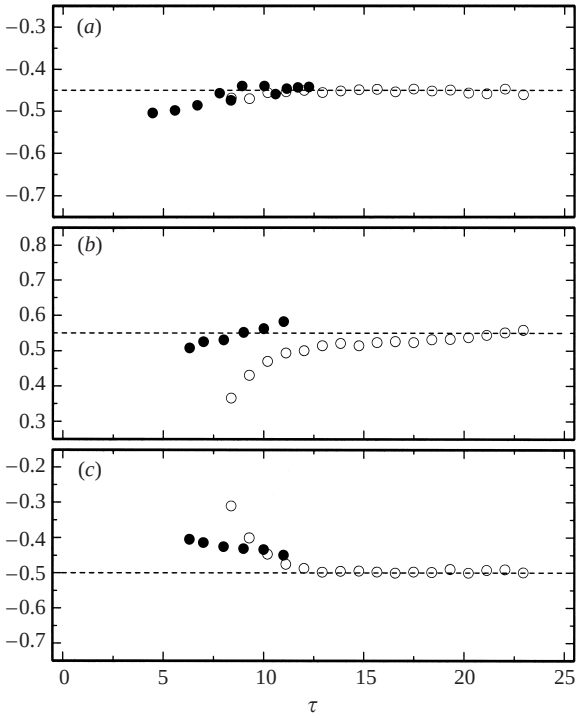

FIGURE 5. Downstream evolution of the correlation coefficients: (*a*) $\overline{u_1 u_2}/u_1' u_2'$, (*b*) $\overline{u_1 \theta}/u_1' \theta'$ and (*c*) $\overline{u_2 \theta}/u_2' \theta'$: ○, present measurements; ●, TC; dashed lines have been plotted only as an aid to the eye.

At this point is seems worthwhile to revisit the TC measurements of turbulent stresses and scalar variance, which have been plotted in figure 4(*b*) The two turbulent stresses could be fitted by exponential functions in the range $8.4 < \tau < 12.3$, with essentially identical exponents (0.130 for the streamwise stress and 0.127 for the transverse stress). On the other hand, the temperature variance in the TC experiments could not be fitted by an exponential expression and its local rate of growth within the entire measuring range was substantially lower than the turbulence growth rate. The most likely explanation for this discrepancy is that the initial level of temperature fluctuations produced by the TC heating system (heating rods, rather than the thin ribbons used in the present setup) was so high that it would require a much larger development time for the asymptotic law, equation (6), to apply. The persisting tendency towards an increase of the growth rate is demonstrated by the TC measurements, in conformity with this hypothesis. The apparent 'immaturity' of the TC temperature fluctuation field, as far as its growth rate is concerned, is not necessarily a problem, because it has been amply demonstrated that, in uniformly sheared flows, structural parameters, such as correlation coefficients, and the fine structure are quick to adjust to their asymptotic states. For example, the low-shear experiments of Champagne, Harris & Corrsin (1970) resulted in stresses that did not achieve exponential growth within the available test section; however, the turbulence anisotropies in these experiments achieved values that were not very different from those in the higher-shear TC experiments. Similar observations were made by Holloway & Tavoularis (1992) concerning the turbulence response to the introduction of

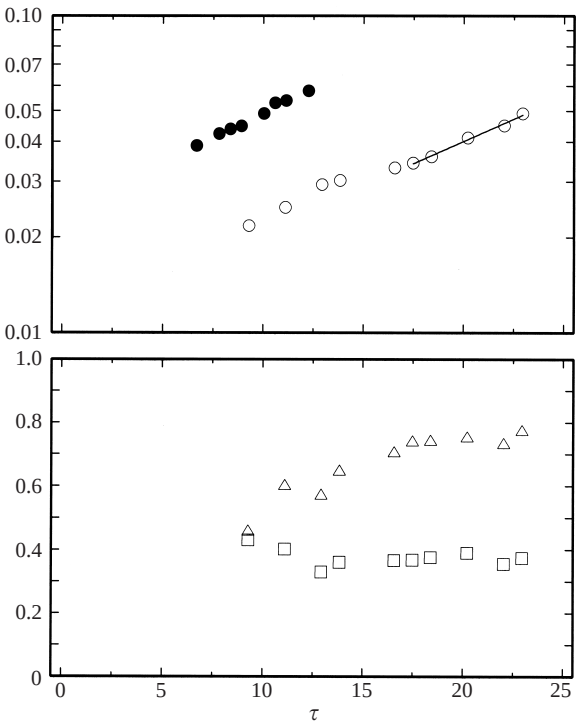

FIGURE 6. Downstream evolution of integral lengthscales: ○, $L_{11,1}$, present measurements, in mm; ●, $L_{11,1}$, TC measurements, in mm; □, $L_{22,1}/L_{11,1}$; △, $L_{\theta 1}/L_{11,1}$.

a constant streamline curvature. A comparison of dimensionless parameters in the present and the TC experiments (table 1) also shows that exponential growth of the scalar variance is not necessarily a prerequisite for the scalar–turbulence interactions and, particularly, the scalar fine structure to reach asymptotic behaviour.

The centreline shear stress correlation coefficient $\overline{u_1 u_2}/u_1' u_2'$ and the heat flux coefficients $\overline{u_1\theta}/u_1'\theta'$ and $\overline{u_2\theta}/u_2'\theta'$, shown in figure 5, all achieved nearly constant values in a large part of the facility, which started significantly upstream of the region over which second moments grew exponentially. Compared to the present results, the corresponding TC measurements, plotted on the same figure, show excellent agreement for the shear stress (in both cases about -0.45 and reasonable agreement for the heat fluxes (0.56 vs. 0.59 for the former and -0.50 vs. -0.45 for the latter).

Measurements of the streamwise integral lengthscale $L_{11,1}$ (figure 6) could be fitted, for $17.5 < \tau < 23.0$, by the exponential law

$$L_{11,1} = 0.0111\,\mathrm{e}^{0.0644\tau}\ \mathrm{mm}.$$

The TC measurements of $L_{11,1}$ also grew nearly exponentially. The integral lengthscale ratios $L_{22,1}/L_{11,1}$ and $L_{\theta 1}/L_{11,1}$, also plotted in figure 6, were nearly constant for $17.5 < \tau < 23.0$, taking asymptotic values of 0.37 and 0.74, respectively, which were comparable to the TC values of 0.33 and 0.76.

The ratio of streamwise Corrsin and Taylor microscales $\lambda_{\theta 1}/\lambda_{11}$ was 0.88, identical to the TC value, while the ratio of the two Corrsin microscales $\lambda_{\theta 1}/\lambda_{\theta 2}$ was 0.66, somewhat lower than the corresponding TC value of 0.73. The inequality of the Corrsin microscales is evidence of a locally anisotropic scalar field.

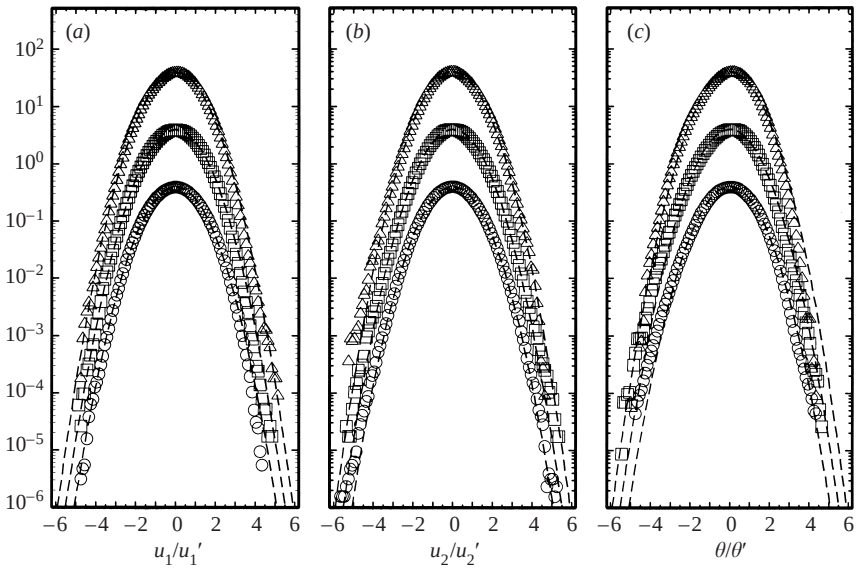

FIGURE 7. Probability density function of the velocity and temperature fluctuations: (*a*) $p(u_1/u_1')$, (*b*) $p(u_2'/u_2')$ and (*c*) $p(\theta/\theta')$; $Re_\lambda = 184$ (○), 200 (□, values multiplied by 10) and 253 (△, values multiplied by 100); dashed lines indicate Gaussian p.d.f.

A point of some concern is that the scalar dissipation rate computed from the balance of equation (5) was 0.80, which is substantially higher than the locally isotropic estimate 0.57, based on the streamwise scalar derivative. The direct measurement of the scalar dissipation rate (assuming that the spanwise mean-square derivative was equal to the transverse one) was also higher than the locally isotropic estimate. This discrepancy may be partially attributed to the local anisotropy of the scalar field. It is interesting to note, however, that the ratios of the different estimates of the scalar dissipation rates were very close to the corresponding values in the TC experiments (table 1).

4.3. *Probability density function*

Figure 7 displays the p.d.f. of the streamwise and transverse velocity fluctuations and scalar fluctuations at three downstream positions corresponding to $Re_\lambda = 184$, 200 and 253. It may be seen that all p.d.f.s were close to the Gaussian one. In particular, the scalar skewness and flatness were, respectively, -0.19 ± 0.06 and 3.15 ± 0.08 over the range of Re_λ considered, only slightly deviating from the Gaussian values. The present results are in general agreement with the TC measurements of p.d.f.s at comparable Re_λ.

As noted in the introduction, there has been some controversy about the shape of the tails of the scalar p.d.f.s. Besides TC, nearly Gaussian scalar p.d.f.s were observed by among others, Thoroddsen & Van Atta (1992) in a stably stratified flow and Overholt & Pope (1996) in their numerical simulation. On the other hand, scalar p.d.f.s with exponential tails were observed in flows with a constant mean scalar gradient by Gollub *et al.* (1991) in a stirred fluid, Jayesh & Warhaft (1991, 1992) in grid turbulence, and Castaing *et al.* (1989) in high Rayleigh number convection. The main conclusion of the latter experimental studies is that there exists a transitional Reynolds number, above which the tails of the scalar p.d.f. would change from Gaussian to exponential. Jayesh & Warhaft (1992) suggested that the transitional

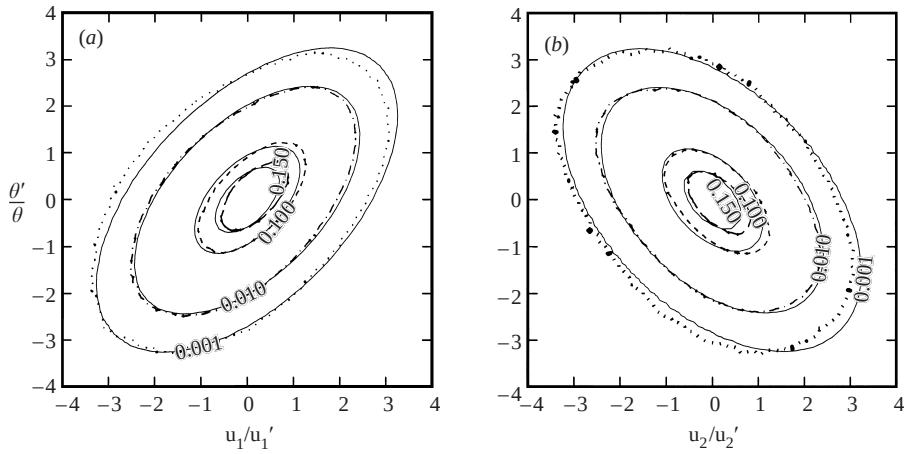

FIGURE 8. Isocontours of the joint p.d.f. of the scalar and (*a*) the streamwise and (*b*) the transverse velocity fluctuations; solid lines indicate the corresponding contours of jointly Gaussian p.d.f. with the same correlation coefficients as the measured ones.

Reynolds number Re_L, based on the integral lengthscale, must be larger than 70. In both the present and the TC experiments, Re_L was much greater than this value (for example, at $Re_\lambda = 253$, $Re_L = 2,380$), without a hint of exponential tails. Furthermore, the lack of exponential tails in the scalar p.d.f.s cannot be attributed to the limited temperature range across the tunnel, because the present mean scalar profile extended over nearly ± 10 scalar standard deviations on either side of the measuring point; for comparison, the mean scalar profile in the Jayesh & Warhaft (1991) experiments extended about ± 6 scalar standard deviations from their centreline. Another argument (Warhaft 2000), that exponential tails of the scalar p.d.f. would only occur if the wind tunnel-cross section extended by at least 8 integral lengthscales, also seems to be contradicted by the present experiments, in which the ratio $h/L_{11,1}$ varied from 14 to 6, while the ratio $h/L_{\theta,1}$ varied from 30 to 8. It may be relevant to mention that Jaberi *et al.* (1996) have concluded that the scalar p.d.f. would depend on the initial conditions and, if a constant mean scalar gradient were imposed, the long-time p.d.f. would become Gaussian.

4.4. *Velocity–scalar joint statistics*

Isocontours of the joint probability density functions of the temperature fluctuations and the streamwise and transverse velocity fluctuations are shown in figure 8. In agreement with the TC findings, both sets of contours displayed only minor differences from the corresponding contours of the jointly normal p.d.f., also shown in the same figure.

The conditional expectations of the velocity fluctuations conditional upon the scalar, appearing in the transport equation of the scalar p.d.f. (equation (9)), have received little attention experimentally and theoretically. Figure 9 displays these parameters, normalized by the corresponding r.m.s. values as well as straight lines with slopes equal to the corresponding correlation coefficients, representing jointly Gaussian random processes. This figure clearly demonstrates that the measured values of both conditional expectations adhered closely to the Gaussian lines, except possibly at large deviations of the scalar fluctuations, for which the experimental uncertainty is also increased. Nearly linear conditional expectations have also been observed by Tong & Warhaft (1995) in a heated jet and by Overholt & Pope (1996) in a

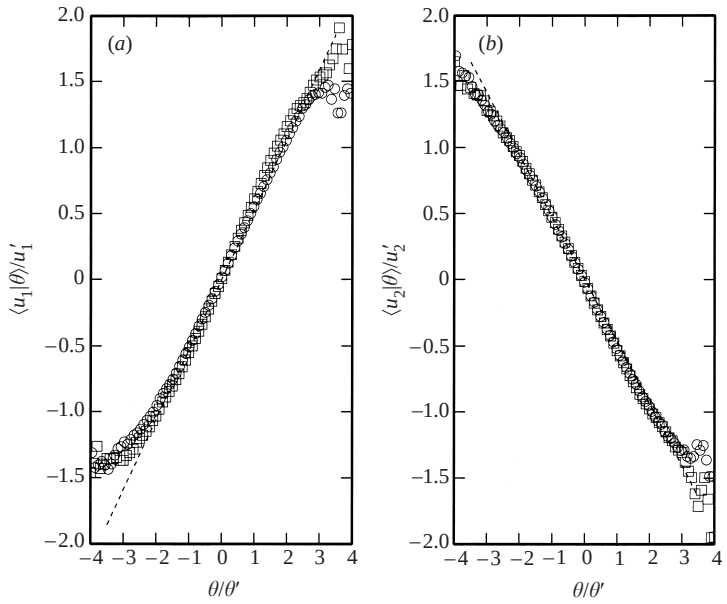

FIGURE 9. Normalized conditional expectations of (*a*) the streamwise and (*b*) the transverse velocity fluctuations, conditioned upon the scalar values; $Re_\lambda = 200$ (○), 253 (□); dashed lines indicated fitted linear expressions.

numerical simulation. Although the linearity of the conditional expectations does not necessarily guarantee Gaussianity (Adrian *et al.* 1989), linearity is consistent with the observed Gaussianity of the scalar p.d.f. and supports the previously presented analytical solution for this p.d.f.

4.5. *Statistics of scalar derivatives and differences*

In contrast to the scalar fluctuations which were essentially Gaussian, the streamwise and transverse derivatives of the scalar were strongly non-Gaussian, as shown by their p.d.f. in figure 10. Both p.d.f.s displayed a very sharp peak and exponential-like tails, which are indicative of internal intermittency of the scalar field. The difference between the two p.d.f.s resides in their asymmetry: the p.d.f. of $\partial\theta/\partial x_1$ had a negative tail which was more flared than the positive one, whereas the opposite is observed in the p.d.f. of $\partial\theta/\partial x_2$.

Concerning the shape of the derivative p.d.f. tails, Holzer & Siggia (1994) suggested an exponential fit as $p_{\partial\theta/\partial x_1} = \exp(-\beta\,|\partial\theta/\partial x_1|^\alpha)$. Because these authors considered isotropic turbulence, their p.d.f. was symmetrical, with equal values of the coefficients $\beta = 2.5$ and $\alpha = 0.66$, for both the negative and the positive tails. In the present case, the streamwise and transverse scalar derivative p.d.f.s were skewed and had asymmetrical tails, thus requiring a different fit to each tail of each p.d.f. Such fittings suggested that $\beta = 1.9$ and $\alpha = 0.78$ for the negative tail and $\beta = 2.1$ and $\alpha = 0.82$ for the positive tail of the p.d.f. of $\partial\theta/\partial x_1$. The corresponding values for the p.d.f. of $\partial\theta/\partial x_2$ were $\beta = 2.0$ and $\alpha = 0.87$ for the negative tail and $\beta = 1.9$ and $\alpha = 0.72$ for the positive tail. The significance of the small differences among the present values and those reported by the Holzer & Siggia (1994) is hard to evaluate.

The opposite asymmetries of the p.d.f.s of $\partial\theta/\partial x_1$ and $\partial\theta/\partial x_2$, also reflected by the opposite signs of their skewness factors, requires some explanation. The shape of $p_{\partial\theta/\partial x_1}$ suggests that contributions from rare but large negative fluctuations of

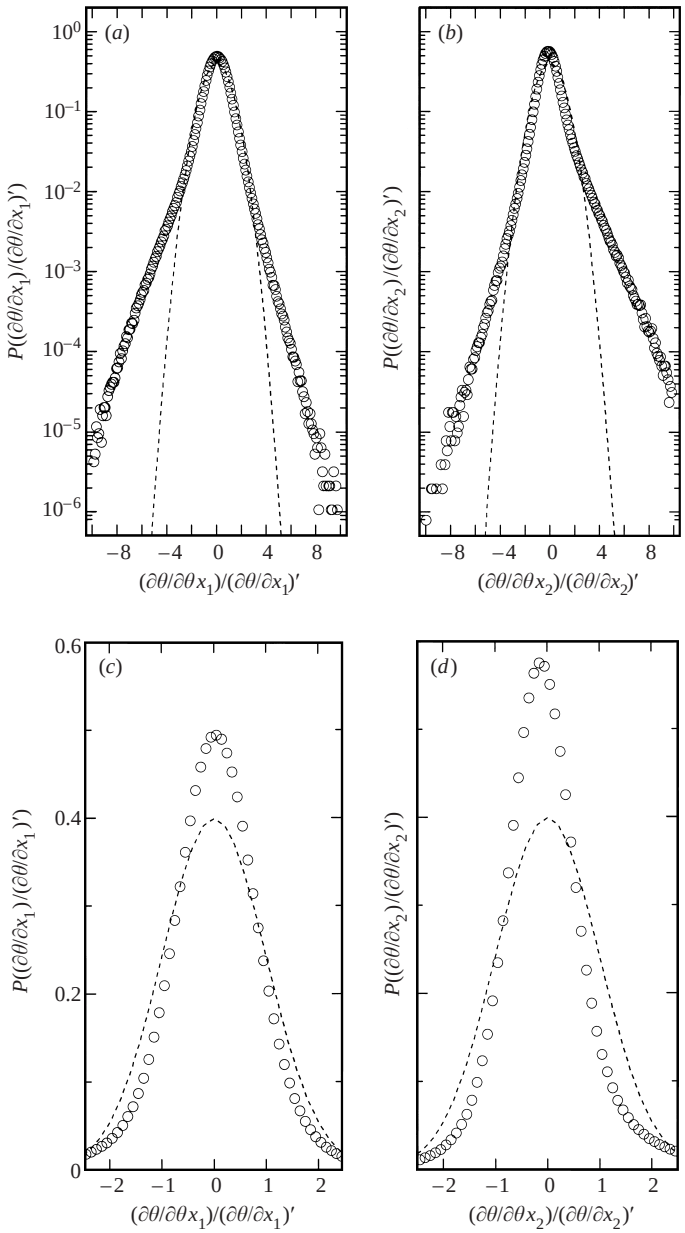

FIGURE 10. Probability density function of (a, c) the streamwise and (b, d) the transverse scalar derivatives; dashed lines indicate Gaussian p.d.f.; (a) and (b) show the entire measured p.d.f. in semilogarithmic axes, while (c) and (d) show the central portions of the same p.d.f. in linear axes.

$\partial\theta/\partial x_1$ dominate those from large positive fluctuations, while the opposite may hold for $p_{\partial\theta/\partial x_2}$. Within the narrow range of Re_λ investigated, the measured skewness of $\partial\theta/\partial x_1$ was nearly constant and equal to -1.0. This value is very close to the TC value of -0.95 and within the scatter of data compiled by Sreenivasan & Antonia (1997) from different shear flows. Non-zero skewness is evidence of local anisotropy. The flatness of $\partial\theta/\partial x_1$ was approximately 19 within the Re_λ range covered. This value was slightly higher than the value of 15 reported by TC but compares well

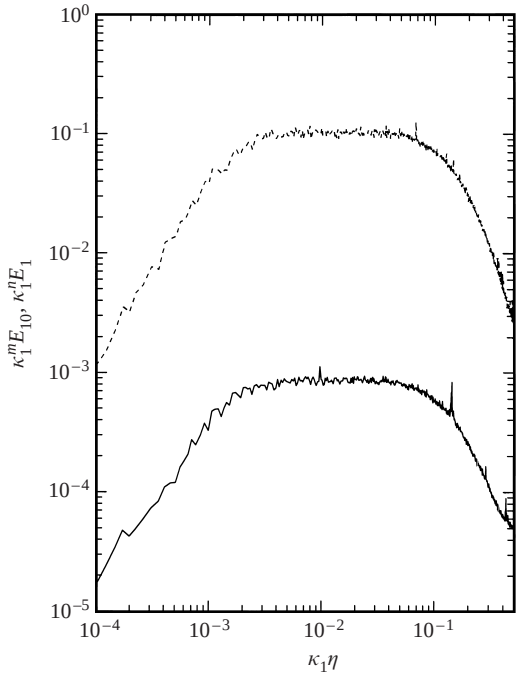

FIGURE 11. Compensated frequency spectra of the scalar (— — —) and the streamwise velocity (———); the ordinate is in arbitrary units.

with the data reported by Sreenivasan & Antonia (1997). One may also note that, at a comparable Re_λ, the flatness of $\partial u_1/\partial x_1$ was much smaller (about 6.3, Ferchichi & Tavoularis 2000), suggesting that the scalar field is more intermittent than the velocity field.

Statistics of $\partial\theta/\partial x_2$ were determined at a single location on the centreline of the wind tunnel, at which $Re_\lambda = 200$. The skewness of this parameter was about 1.5, comparable to measurements in other shear flows (TC; Sreenivasan *et al.* 1977; Mestayer 1982). We point out, however, that values of this skewness measured in grid turbulence with a constant mean scalar gradient were higher than those obtained in shear flows. Tong & Warhaft (1994), Holzer & Siggia (1994) and Pumir (1994) found this skewness to be about 1.9, independently of Re_λ. Tong & Warhaft (1994) suggested that large skewness in shearless turbulent flows is associated with the strong correlation between u_2 and θ in such flows. The flatness of $\partial\theta/\partial x_2$ was about 13, comparable to the values of 11 by TC and 10 by Mestayer (1982) in a turbulent boundary layer at $Re_\lambda = 616$. At a comparable Re_λ, the flatness of $\partial u_1/\partial x_2$ was found to be about 8 (Ferchichi & Tavoularis 2000), considerably smaller than the scalar derivative flatness, conforming with previous observations that the scalar field is more intermittent than the velocity field.

4.6. *Inertial-range measurements*

Figure 11 is a plot of the one-dimensional spectra of the streamwise velocity, $E_{11}(\kappa_1)$, and the scalar fluctuations $E_\theta(\kappa_1)$, vs. the dimensionless streamwise wavenumber $\kappa_1\eta = 2\pi f\eta/U_c$ (f is the frequency; $Re_\lambda = 253$). Both spectra are shown multiplied by powers of κ_1, with the exponents selected such as to present the longest possible plateaux, which presumably define the inertial range. The most suitable values of the

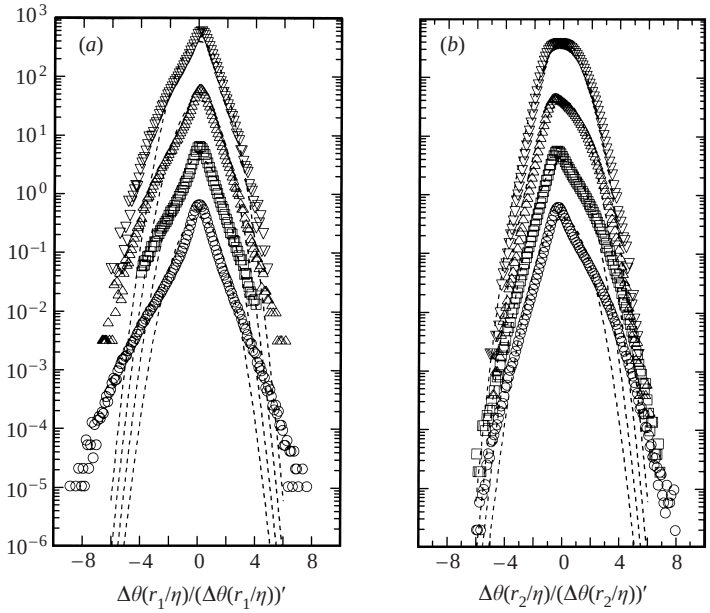

FIGURE 12. Probability density function of scalar differences for (*a*) streamwise separations, $r_1/\eta = 20$ (○), 40 (□), 60 (△) and 100 (▽), and (*b*) transverse separations, $r_2/\eta = 26$ (○), 37 (□), 79 (△) and 156 (▽); $Re_\lambda = 200$; for clarity, each of the last three plots in each graph has been shifted upwards from the previous plot by one decade.

exponents were found to be $n = 1.50$ for the velocity spectrum and $m = 1.24$ for the scalar spectrum. Both values are lower than the Kolmogorov value of 5/3, with the scalar spectrum being more distant from the Kolmogorov value. The extents of both inertial ranges were about 1.5 decades, although the scalar inertial range was slightly narrower than the velocity one.

Figure 12 presents plots of the p.d.f. of the streamwise and transverse scalar differences, for varying separations r_i/η within the inertial range. It can be seen from these plots that, even for relatively large separation distances, the p.d.f.s have sharp peaks and exponential-like tails, consistently with the expected intermittency of the scalar field in the inertial range. This is corroborated by the plots of the corresponding flatness of the scalar differences (figure 13), which decreased, at large separation distances, from the flatnesses of the corresponding derivatives towards the Gaussian value 3.0. This suggests that the scalar internal intermittency became more pronounced as the separation distance decreased. Note that, for all r_i/η, the measured flatness of the streamwise scalar difference was higher than that of the transverse scalar difference. Figure 13 also includes plots of the flatness of the streamwise velocity differences at Re_λ comparable to those of the scalar plots. In all cases the scalar flatness was significantly higher than the corresponding velocity flatness, pointing to a higher intermittency of the scalar field. Finally, figure 14 shows the skewnesses of the streamwise and transverse scalar differences for varying r_i/η. Both decreased monotonically with increasing r_i/η, in conformity with the trends observed by Mydlarski & Warhaft (1998). An interesting observation is that, although the magnitude of the skewness of the scalar differences for streamwise separations lower than a certain value ($r_i/\eta < 80$ for $Re_\lambda = 200$) was higher than that for the same value of transverse separation, the opposite was observed for higher r_i/η; apparently,

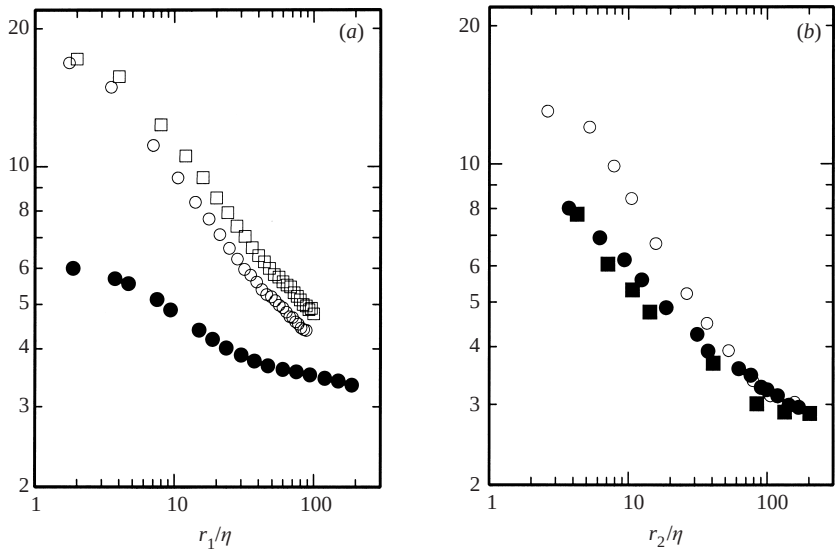

FIGURE 13. Measurements of the flatness factors of the velocity (solid symbols) and scalar (open symbols) differences for (*a*) streamwise and (*b*) transverse separations; $Re_\lambda = 172$ (■), 200 (○), 253 (□) and 264 (●).

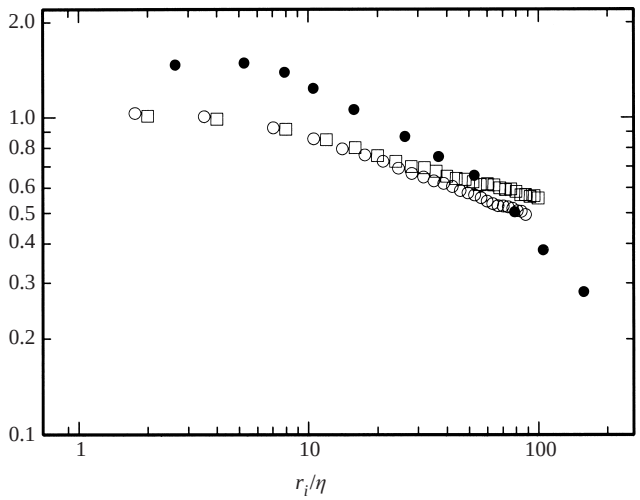

FIGURE 14. Measurements of the skewness (in magnitude only) of scalar differences for streamwise separations ($Re_\lambda = 200$ (○) and 253 (□)) and transverse separations ($Re_\lambda = 200$ (●)).

this is related to the fact that integral lengthscales in the streamwise direction are larger than those in the transverse direction.

4.7. *Joint statistics of the scalar and its dissipation rate*

Local isotropy requires that the fine structure of the scalar field should be statistically independent of the motions that contribute mostly to the scalar variance. A necessary, although not sufficient, condition for independence is the vanishing of the correlation

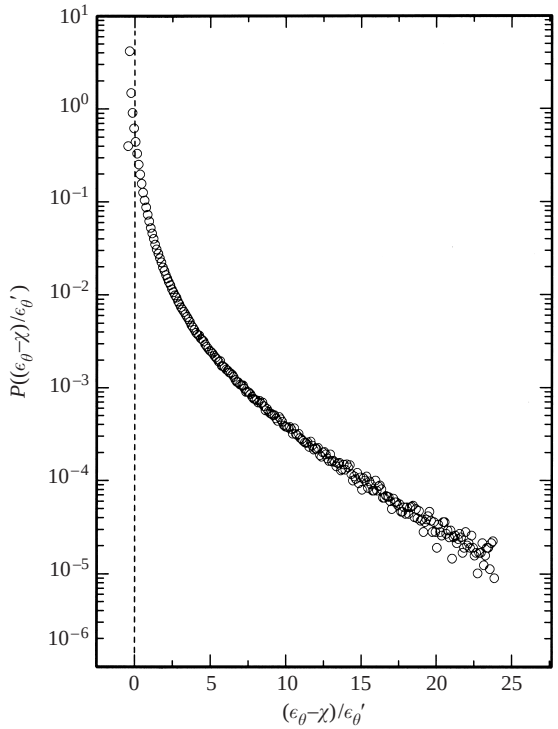

FIGURE 15. Probability density function of the scalar dissipation rate; $Re_\lambda = 253$.

coefficient between the scalar fluctuations and their destruction rate (Jayesh & Warhaft 1992)

$$\rho_{\theta^2\epsilon_\theta} = \frac{\overline{(\theta^2 - \overline{\theta^2})(\epsilon_\theta - \chi)}}{\overline{(\theta^2 - \overline{\theta^2})^2}^{1/2}\overline{(\epsilon_\theta - \chi)^2}^{1/2}}.$$

This correlation coefficient was measured by approximating the mean thermal destruction rate by its locally isotropic expression χ_{li} based on the streamwise scalar derivative. For all cases examined, this correlation coefficient was, in magnitude, less than 0.02, which is sufficiently low for the necessary condition for independence to apply.

Further insight into the statistical independence of θ and ϵ_θ can be inferred by evaluating their coherence function, defined as the cross-spectrum of these parameters normalized by the square roots of the corresponding frequency spectra. The magnitude of this coherence function (not shown here), measured at $Re_\lambda = 200$ and 253, up to a frequency equal to twice the frequency corresponding to the Taylor microscale (thus more than covering the inertial range) was less than 0.02 within the examined frequency range. This is further indication that θ and ϵ_θ are essentially independent in the present flow configuration.

A stronger test of the statistical independence of θ and ϵ_θ may be made by considering their joint p.d.f. Statistical independence requires that

$$p(\theta, \epsilon_\theta) = p(\theta)p(\epsilon_\theta). \tag{19}$$

Figure 15 displays the p.d.f. of ϵ_θ (based on the streamwise scalar derivative) and indicates that, although values near the average have the highest probability, large

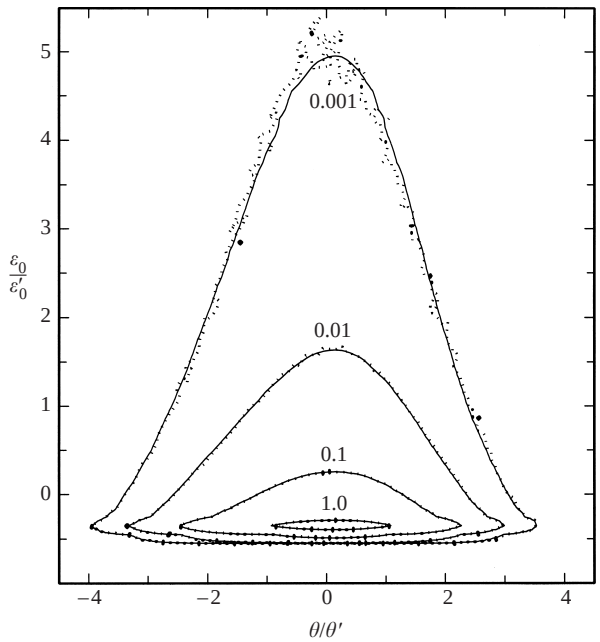

FIGURE 16. Comparison of four isocontours of the joint p.d.f. of the scalar and its dissipation rate (scattered dots) and the corresponding isocontours of the product of the p.d.f. of the scalar and the p.d.f. of its dissipation rate (continuous lines); numbers in the graph indicate the values of the p.d.f. for each pair of isocontours.

positive fluctuations in ϵ_θ, up to 25 times its standard deviation, also occur, but with low probability. Iso-probability contours of $p(\theta, \epsilon_\theta)$ are displayed in figure 16. These contours are nearly symmetrical with respect to the mean of the scalar fluctuations, suggesting that the fluid is well mixed and that the scalar dissipation gets nearly equal contributions from the negative and the positive scalar fluctuations. Contours of the product $p(\theta)p(\epsilon_\theta)$, also plotted in figure 16, essentially collapsed on the corresponding contours of $p(\theta, \epsilon_\theta)$, which validates equation (19) and, hence, proves the independence of θ and ϵ_θ.

Another quantity of interest is the conditional expectation of the scalar dissipation rate $\langle \epsilon_\theta | \theta \rangle$, conditional upon the scalar, which appears in the transport equation of the scalar p.d.f. (equation (10)). Measurements of this parameter, shown in figure 17 in the usual normalized form, were within $\pm 10\%$ of 1.0 for $|\theta/\theta'| < 2$, although displaying substantial scatter for $|\theta/\theta'| > 2$. The level of scatter is consistent with the number of experimental values used to calculate each value of $\langle \epsilon_\theta | \theta \rangle$: about 400 000 points at $\theta/\theta' = 0$, but only a few hundred points at $\theta/\theta' = \pm 4$. Uncertainty bars have been added to the set of data that displays the largest scatter. The limit values of these bars enclose, at the 95% confidence level, the ranges of average values of $\langle \epsilon_\theta | \theta \rangle$ at a given θ/θ' that would most likely be obtained if the data populations contained infinite samples. It is clear that $\langle \epsilon_\theta | \theta \rangle / \chi \simeq 1$ within the measurement uncertainty.

Based on the above tests, it seems reasonable to conclude that the conditional expectation of the scalar dissipation rate in uniformly sheared turbulence is independent of the scalar value. As discussed in the introduction, such independence has also been observed in several other well-mixed homogeneous and non-homogeneous turbulent

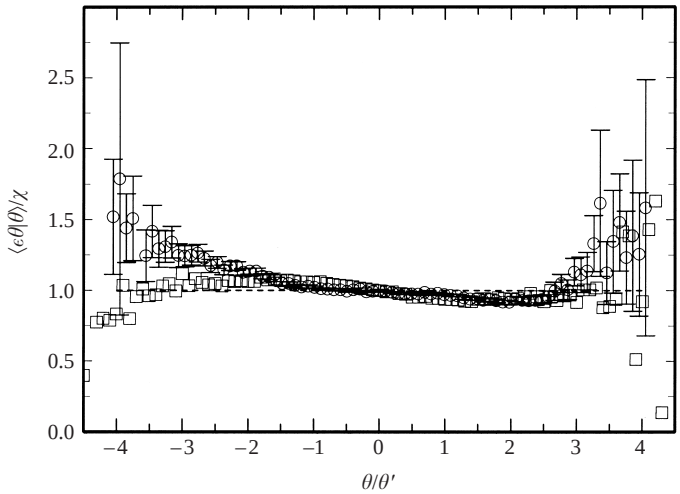

FIGURE 17. Conditional expectation of the scalar dissipation rate, conditioned upon the scalar value; $Re_\lambda = 200$ (○) and 253 (□); error bars have been added to the $Re_\lambda = 200$ data.

flows, both experimentally and computationally (e.g. Anselmet *et al.* 1994; Mi *et al.* 1995; Overholt & Pope 1996). A departure from this conclusion is the measurements of ϵ_θ by Jayesh & Warhaft (1992), which displayed a V-shape when conditioned upon the scalar.

5. Conclusions

The objective of the present study was to examine in detail the probability density function and the fine structure of a scalar field that was introduced passively in uniformly sheared turbulent flow. The flow configuration was essentially the same as the one studied by Tavoularis & Corrsin (1981*a*, *b*), with a uniform mean temperature gradient imposed on the flow by heating electric elements. An advantage over the TC flow was the generation of a higher shear parameter, resulting in more vigorous turbulence production, a higher turbulence intensity and a nearly double total mean strain on the turbulence in the measuring section. Another advantage was the use of fine heating ribbons, rather than heating rods, which introduced a milder initial scalar injection. This, in combination with the stronger scalar fluctuation production, resulted in a complete decoupling of the scalar field from its initial condition and allowed the scalar fluctuations to grow in a self-similar fashion and at the same exponential rate as the turbulence, as predicted by an analytical solution of the scalar variance equation. Other than that, however, the structures of the turbulence and the scalar field were quite comparable to those in the TC experiments; both flows were at comparable turbulence Reynolds numbers, in the vicinity of 250.

An analytical examination of the scalar p.d.f. equation in uniformly sheared flow with a constant mean scalar gradient, taking into consideration some experimental evidence, has concluded that the scalar p.d.f. must be Gaussian. Measurements of the scalar p.d.f. also clearly indicate that it was essentially Gaussian. The joint p.d.f.s of the scalar and the velocity fluctuations were also essentially jointly Gaussian, with the conditional expectations of the velocity fluctuations linearly dependent on the scalar value.

Probability density functions of scalar derivatives in both the streamwise and

the transverse directions were strongly non-Gaussian and skewed, displaying flared, asymmetric tails. Probability density functions of scalar differences for separations in the inertial range were also strongly non-Gaussian. All measurements in both the dissipative and the inertial ranges point to a highly intermittent scalar fine structure, and, in fact, more intermittent than the fine structure of the turbulence. Finally, joint statistics of the scalar and its dissipation rate demonstrate a statistical independence of the two parameters.

It is hoped that the present findings will help clarify the contested hypotheses that have been put forward to describe the p.d.f. and the fine structure of passive scalars mixed by turbulent shear flows.

Financial support has been provided by the Natural Sciences and Engineering Research Council of Canada. We thank Professor Stephen B. Pope for helping us to prove the uniqueness of the Gaussian function as a solution of equation (17).

REFERENCES

Abramowitz, M. & Stegun, I. A. (Eds.) 1972 *Handbook of Mathematical Functions with Formulas, Graphs and Mathematical Tables*. Wiley-Interscience.

Adrian, R. J., Jones, B. G., Chung, M. K., Hassan, Y., Nithianandan, C. K. & Tung, A. T.-C. 1989 Approximation of turbulent conditional averages by stochastic estimation. *Phys. Fluids* A **1**, 992.

Anselmet, F., Djeridi, H. & Fulachier, L. 1991 Joint statistics between a passive scalar and its dissipation in a turbulent boundary layer. In *Proc. 8th Symp. on Turbulent Shear Flow, Munich*, 27-3.

Anselmet, F., Djeridi, H. & Fulachier, L. 1994 Joint statistics between a passive scalar and its dissipation in turbulent flows. *J. Fluid Mech.* **280**, 173.

Antonia, R. A. & Browne, L. W. B. 1986 Anisotropy of the temperature dissipation in a turbulent wake. *J. Fluid Mech.* **163**, 393.

Antonia, R. A. & Mi, J. 1993 Temperature dissipation in a turbulent round jet. *J. Fluid Mech.* **250**, 531.

Antonia, R. A., Ould-Rouis, M., Anselmet, F. & Zhu, Y. 1997 Analogy between predictions of Kolmogorov and Yaglom. *J. Fluid Mech.* **332**, 395.

Antonia, R. A., Zhu, Y., Anselmet, F. & Ould-Rouis, M. 1996 Comparison between the sum of second-order velocity structure functions and the second-order temperature structure function. *Phys. Fluids* **8**, 3105.

Browne, L. W. B. & Antonia, R. A. 1987 The effect of wire length on temperature statistics in a turbulent wake. *Exps. Fluids* **5**, 426.

Castaing, B., Gunaratne, G., Heslot, F., Kadanoff, L., Libchaber, A., Thomae, S., Wu, X. Z., Zaleski S. & Zanetti, G. 1989 Scaling of hard thermal turbulence in Rayleigh–Benard convection. *J. Fluid Mech.* **204**, 1.

Champagne, F. H., Harris, V. G. & Corrsin, S. 1970 Experiments on nearly homogeneous turbulence. *J. Fluid Mech.* **41**, 81.

Chen, H., Chen, S. & Kraichnan, R. H. 1989 Probability distribution of a stochastically advected scalar field. *Phys. Rev. Lett.* **63**, 2657.

Chen, S., Doolen, G. D., Kraichnan, R. H. & She, Z. S. 1993 On statistical correlations between velocity increments and locally averaged dissipation in homogeneous turbulence. *Phys. Fluids* A **5**, 458.

Ching, E. S. C. & Tsang, Y. K. 1997 Passive scalar conditional statistics in a model of random advection. *Phys. Fluids* **9**, 1353.

Corrsin, S. 1951 On the spectrum of isotropic temperature fluctuations in isotropic turbulence. *J. Appl. Phys.* **22**, 469.

Dopazo, C. 1976 A probabilistic approach to turbulent mixing of reactive scalars. *Third Symp. on Atmospheric Turbulence, Diffusion and Air Quality*. American Meteorological Society, Boston.

Dopazo, C. & O'Brien, E. E. 1974 An approach to the autoignition of a turbulent mixture. *Acta Astron.* **1**, 1239.

Dopazo, C. & O'Brien, E. E. 1975 Functional formulation of nonisothermal turbulent reactive flows. *Phys. Fluids* **17**, 1968.

Eswaran, V. & Pope, S. B. 1988 Direct numerical simulations of the turbulent mixing of a passive scalar. *Phys. Fluids* **31**, 506.

Ferchichi, M. 2000 Measurements of small-scale statistics and probability density functions in passively heated shear flow. PhD Dissertation, Department of Mechanical Engineering, University of Ottawa.

Ferchichi, M. & Tavoularis, S. 2000 Reynolds number effects on the fine structure of uniformly sheared turbulence. *Phys. Fluids* **12**, 2942.

Frisch, U. 1995 *Turbulence*. Cambridge University Press.

Gao, F. 1991 Mapping closure and non-Gaussianity of the scalar probability density functions in isotropic turbulence. *Phys. Fluids* A **3**, 2438.

Gao, F. & O'Brien, E. E. 1991 A mapping closure for multispecies Fickian diffusion. *Phys. Fluids* A **3**, 956.

Gibson, C. H., Friehe, C. A. & McConnell, S. O. 1977 Structure of sheared turbulent fields. *Phys. Fluids* **20**, S156.

Gollub, J. P., Clarke, J., Gharib, M., Lane, B. & Mesquita, O. N. 1991 Fluctuations and transport in a stirred fluid with a mean gradient. *Phys. Rev. Lett.* **67**, 3507.

Holloway, A. G. L. & Tavoularis, S. 1992 The effects of curvature on sheared turbulence. *J. Fluid Mech.* **237**, 569.

Holzer, M. & Pumir, A. 1993 Simple models of non-Gaussian statistics for a turbulently advected passive scalar. *Phys. Rev.* E **47**, 202.

Holzer, M. & Siggia, E. D. 1994 Turbulent mixing of a passive scalar. *Phys. Fluids* **6**, 1820.

Jaberi, F. A., Miller, R. S., Madnia, C. K. & Givi, P. 1996 Non-Gaussian scalar statistics in homogeneous turbulence. *J. Fluid Mech.* **313**, 241.

Jayesh, Tong, C. & Warhaft, Z. 1994 On temperature spectra in grid turbulence. *Phys. Fluids* **6**, 306.

Jayesh & Warhaft, Z. 1991 Probability distribution of a passive scalar in grid-generated turbulence. *Phys. Rev. Lett.* **67**, 3503.

Jayesh & Warhaft, Z. 1992 Probability distribution, conditional dissipation, and transport of passive temperature fluctuations in grid-generated turbulence. *Phys. Fluids* A **4**, 2292.

Kailasnath, P., Sreenivasan, K. R. & Saylor, J. R. 1993 Conditional scalar dissipation rates in turbulent wakes, jets, and boundary layers. *Phys. Fluids* A **5**, 3207.

Karnik, U. & Tavoularis, S. 1987 Generation and manipulation of uniform shear with the use of screens. *Exps. Fluids* **5**, 255.

Karnik, U. & Tavoularis, S. 1989 Measurements of heat diffusion from a continuous line source in a uniformly sheared turbulent flow. *J. Fluid Mech.* **202**, 233.

Kerr, R. M. 1985 Higher-order derivative correlations and the alignment of small scale structures in isotropic numerical turbulence. *J. Fluid Mech.* **153**, 31.

Kerstein, A. R. & McMurtry, P. A. 1994 Mean-field theories of random advection. *Phys. Rev.* E **49**, 474.

Kolmogorov, A. N. 1941 Local structure of turbulence in an incompressible fluid for very large Reynolds numbers. *Dokl. Akad. Nauk SSSR* **30**, 299.

Lundgren, T. S. 1967 Distribution functions in the statistical theory of turbulence. *Phys. Fluids* **10**, 969.

Mestayer, P. 1982 Local isotropy and anisotropy in a high-Reynolds-number turbulent boundary layer. *J. Fluid Mech.* **125**, 475.

Mi, J., Antonia, R. A. & Anselmet, F. 1995 Joint statistics between temperature and its dissipation rate components in a round jet. *Phys. Fluids* **7**, 1665.

Mydlarski, L. & Warhaft, Z. 1998 Passive scalar statistics in high-Péclet-number grid turbulence. *J. Fluid Mech.* **358**, 135.

O'Brien, E. E. & Jiang, T. L. 1991 The conditional dissipation rate of an initially binary scalar in homogenous turbulence. *Phys. Fluids* A **3**, 3121.

Obukhov, A. M. 1949 Structure of the temperature field in turbulent flow. *Izv. Akad. Nauk SSSR, Geogr. i Geofiz.* **13**, 58.

Overholt, M. R. & Pope, S. B. 1996 Direct numerical simulation of a passive scalar with imposed mean gradient in isotropic turbulence. *Phys. Fluids* **8**, 3128.

Pope, S. B. 1976 The probability approach to the modeling of turbulent reacting flows. *Combust. Flame* **27**, 299.

Pope, S. B. 1985 Pdf methods for turbulent reactive flows. *Prog. Energy Combust. Sci.* **11**, 119.

Pumir, A. 1994 A numerical study of the mixing of a passive scalar in three dimensions in the presence of a mean gradient. *Phys. Fluids* **6**, 2118.

Pumir, A., Shraiman, B. & Siggia, E. D. 1991 Exponential tails and random advection. *Phys. Rev. Lett.* **66**, 2984.

Sahay, A. & O'Brien, E. 1993 Uniform mean scalar gradient in grid turbulence: Conditioned dissipation and production. *Phys. Fluids* A **5**, 1076.

Sinai, Y. G. & Yakhot, V. 1989 Limiting probability distributions of a passive scalar in a random velocity field. *Phys. Rev. Lett.* **63**, 1962.

Sreenivasan, K. R. 1991 On local isotropy of passive scalars in turbulent shear flows. *Proc. R. Soc. Lond.* A **434**, 165.

Sreenivasan, K. R. & Antonia, R. A. 1997 The phenomenology of small-scale turbulence. *Annu. Rev. Fluid Mech.* **29**, 435.

Sreenivasan, K. R., Antonia, R. A. & Britz, D. 1979 Local isotropy and large structures in a heated turbulent jet. *J. Fluid Mech.* **94**, 745.

Sreenivasan, K. R., Antonia, R. A. & Danh, H. Q. 1977 Temperature dissipation fluctuations in a turbulent boundary layer. *Phys. Fluids* **20**, 1238.

Sreenivasan, K. R. & Tavoularis, S. 1980 On the skewness of the temperature derivative in turbulent flows. *J. Fluid Mech.* **101**, 783.

Tavoularis, S. 1985 Asymptotic laws of transversely homogeneous turbulent shear flows. *Phys. Fluids* **28**, 999.

Tavoularis, S. & Corrsin, S. 1981*a* Experiments in nearly homogenous turbulent shear flow with a uniform mean temperature gradient. Part 1. *J. Fluid Mech.* **104**, 311.

Tavoularis, S. & Corrsin, S. 1981*b* Experiments in nearly homogenous turbulent shear flow with a uniform mean temperature gradient. Part 2. The fine structure. *J. Fluid Mech.* **104**, 349.

Tavoularis, S. & Karnik, U. 1989 Further experiments on the evolution of turbulent stresses and scales in uniformly sheared turbulence. *J. Fluid Mech.* **204**, 457.

Tavoularis, S. & Sreenivasan, K. R. 1981 Skewness of the temperature derivative in an asymmetrically heated wake. *Phys. Fluids* **24**, 778.

Thoroddsen, S. T. & Van Atta, C. W. 1992 Exponential tails and skewness of density-gradient probability density functions in stably stratified turbulence. *J. Fluid Mech.* **244**, 547.

Thoroddsen, S. T. & Van Atta, C. W. 1996 Experiments on density-gradient anisotropies and scalar dissipation of turbulence in a stably stratified fluid. *J. Fluid Mech.* **322**, 383.

Tong, C. & Warhaft, Z. 1994 On passive scalar derivative statistics in grid turbulence. *Phys. Fluids* **6**, 2165.

Tong, C. & Warhaft, Z. 1995 Passive scalar dispersion and mixing in a turbulent jet. *J. Fluid Mech.* **292**, 1.

Valiño, L. 1995 Multiscalar mapping closure for mixing in homogeneous turbulence. *Phys. Fluids* **7**, 144.

Valiño, L., Dopazo, C. & Ros, J. 1994 Quasistationary probability density functions in the turbulent mixing of a scalar field. *Phys. Rev. Lett.* **72**, 3518.

Warhaft, Z. 2000 Passive scalars in turbulent flows. *Annu. Rev. Fluid Mech.* **32**, 203.

Wyngaard, J. C. 1971 Spatial resolution of a resistance wire temperature sensor. *Phys. Fluids* **14**, 2052.

Yakhot, V. 1989 Probability distributions in high-Rayleigh-number Bénard convection. *Phys. Rev. Lett.* **63**, 1965.